Diamond & Related Materials 136 (2023) 109935

Contents lists available at ScienceDirect

Diamond & Related Materials

journal homepage: www.elsevier.com/locate/diamond

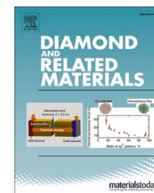

# Dependence of piezoresistive behavior upon Cu content in Cu-DLC nanocomposite films

Chunliang Yan [a,c], Peng Guo [a,*], Jingyuan Zhou [a], Rende Chen [a], Aiying Wang [a,b,**]

[a] Key Laboratory of Marine Materials and Related Technologies, Zhejiang Key Laboratory of Marine Materials and Protective Technologies, Ningbo Institute of Materials Technology and Engineering, Chinese Academy of Sciences, Ningbo 315201, China
[b] Center of Materials Science and Optoelectronics Engineering, University of Chinese Academy of Sciences, Beijing 100049, China
[c] School of Materials Science and Engineering, Shanghai University, Shanghai 200444, China

ARTICLE INFO

*Keywords:*
Cu-containing diamond-like carbon
Microstructure
Piezoresistive behavior
Carrier transport mechanism

ABSTRACT

In this work, Cu-containing diamond-like carbon (Cu-DLC) films were deposited using a hybrid system combining an anode-layer ion beam carbon source and DC magnetron sputtering, where the Cu content in range of 1.0–67.7 at.% was controlled by varying sputtering current. The effect of Cu content on the electrical and piezoresistive behavior of films was investigated. Increasing the Cu content from 1.0 to 67.7 at.% enhanced the conductive $sp^2$ phases and caused the more Cu nanoparticulates dispersed uniformly in the insulate $sp^3$ amorphous matrix, which significantly reduced the gauge factor from 5.6 to 1.4. Meantime, the temperature coefficient of resistance demonstrated the increase from −3646 to +294 ppm/K with increasing the temperature from 100 to 350 K, indicating the electrical properties were dominated from typical semiconductor to metal-like behavior. Particularly, increasing Cu content from 20.6 to 67.7 at.% led to the threshold voltage being identified and gradually decreasing. The electrical and piezoresistive behavior of the Cu-DLC films was discussed in terms of the carrier tunneling process between conductive phases distributed in amorphous $sp^3$ matrix.

## 1. Introduction

Metal-containing diamond-like carbon (DLC) films have attracted much attention because of their excellent mechanical, tribological, electrical, and optical properties [1,2]. Recently, combined with a strong piezoresistive effect, the metal-containing DLC films have exhibited great potential as advanced film sensors under harsh environments. To develop high-performance piezoresistive film sensor without additional temperature compensation circuit in a wide temperature range, many researchers have explored various metal-containing DLC to obtain both high piezoresistive gauge factor (GF) and low temperature coefficient of resistance (TCR), including Cu [3], W [4], Ni [5,6], Ag [7,8], Cr [9], Sn [10]. For example, Tamulevičius et al. prepared Ag-containing DLC by plasma assisted methods. Its maximum GF was 16, and TCR reached 2180 ppm/K when Ag content was 0.6 at.%. They pointed out that both GF and TCR depended partly on the Ag content [8]. Meškinis and co-workers observed that both TCR and GF of Cr-containing DLC relied on the size of $sp^2$ clusters, $sp^2/sp^3$, and Cr/C ratio [9]. They also found that the Ni-containing DLC with Ni content less than 3.5 at.% showed a giant negative piezoresistive effect, with GF around −3200 due to the conductive clusters rearranged to form new conductive paths under stress [6]. While Koppert et al. reported that Ni-containing DLC deposited in a wide range of process parameters had GF of 12. With 52 at.% Ni, its TCR was approximately zero in the temperature range of 80– 400 K because of the compensation effect of metal on semiconductor [5].

Essentially, GF and TCR reflect the change of material resistance to strain and temperature separately, both of them depend on carrier transport behavior. While, compared with the crystal semiconductors, amorphous semiconductors have the more complicated carrier transport mechanism because of the localized state of the electrons [11]. Wang et al. discovered that GF of DLC showed a strong dependence on the cluster size and $sp^2$ content, where its bandgap width decreased with decreasing $sp^2$ cluster size [12,13]. With the incorporation of various metals, the structure and carrier transport behavior of the metal-containing DLC became more intricate and complex. For instance,

* Corresponding author.
** Correspondence to: A. Wang, Key Laboratory of Marine Materials and Related Technologies, Zhejiang Key Laboratory of Marine Materials and Protective Technologies, Ningbo Institute of Materials Technology and Engineering, Chinese Academy of Sciences, Ningbo 315201, China.
*E-mail addresses:* guopeng@nimte.ac.cn (P. Guo), aywang@nimte.ac.cn (A. Wang).

https://doi.org/10.1016/j.diamond.2023.109935
Received 13 January 2023; Received in revised form 18 March 2023; Accepted 13 April 2023
Available online 17 April 2023
0925-9635/© 2023 Published by Elsevier B.V.

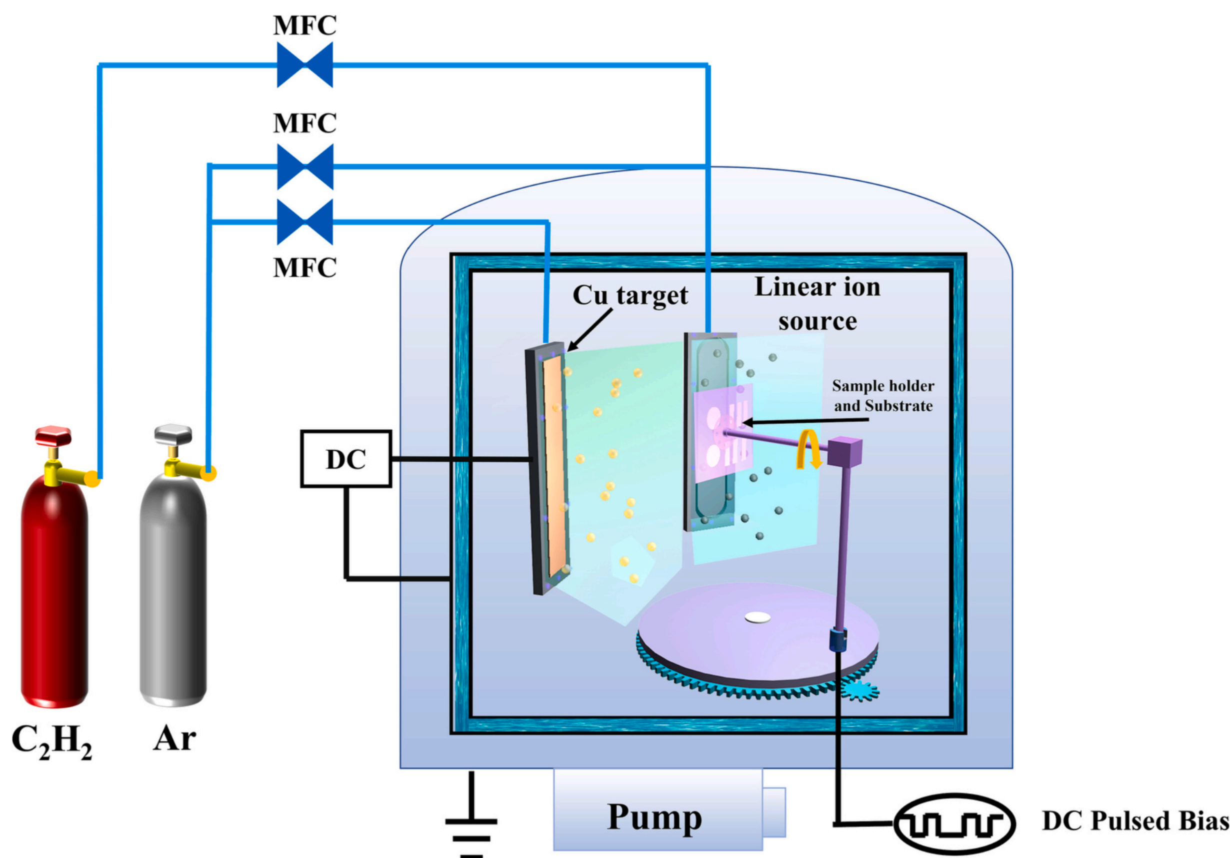


**Fig. 1.** A schematic diagram of hybrid plasma equipment.

Schultes et al. found that the electrical properties of Ni-DLC changed from semiconductor to metal characteristics when the Ni content reached 75 at.% [14]. Tibrewala et al. proposed the thick film resistors (TFR) model to explain the piezoresistive effect in DLC. Furthermore, Meškinis et al. pointed out that the percolation–tunneling model agreed well with the tendencies of GF in metal-containing DLC [3,15]. In general, the $sp^2/sp^3$ ratio, content, and distribution of conductive metal phase change greatly in various metal-containing DLC films. Their influence on the carrier transport behavior and piezoresistive effect is ambiguous, which significantly restricts the development and application of carbon-based piezoresistive film sensors.

In our previous work, we found that the bond characteristic of the highest occupied molecular orbital of Cu and C atoms was antibonding in Cu-containing DLC (Cu-DLC). And the Cu atoms would be dissolved or distributed as metal nanoparticulates in the amorphous carbon matrix [16,17], which meant a simple structure for electrical behavior analysis. In this study, a series of Cu-DLC films with various Cu contents were fabricated, their structural evolution, piezoresistive and electrical properties were studied, and the underlying carrier transport mechanism was also discussed.

## 2. Experimental details

### *2.1. Sample preparation*

Cu-DLC films were deposited by a hybrid plasma process combining an anode-layer ion beam source (ALIS) and DC magnetron sputtering (DCMS). Fig. 1 shows the schematic of deposition system. Acetylene of flow rate at 10 sccm was supplied to ALIS as carbon source. A copper target (400 × 100 × 7 mm with purity of 99.99 wt%) was employed for the Cu sputtering process, where 70 sccm argon was introduced as the sputtering gas. N-type silicon (100), n-type silicon (100) without diffraction peaks in the range of 20–110°, n-type silicon (100) substrates with 300 nm-thick $SiO_2$ film by dry oxidation, high-conductivity silicon, and $Al_2O_3$ (0001) were used as substrates for different characterizations. All substrates were positioned in the deposition chamber, and when the vacuum chamber's pressure reached $2 \times 10^{-5}$ Torr, the substrates were cleaned with $Ar^+$ ions for 20 min to remove any surface contaminants and oxide, with a DC pulsed bias of −100 V. During deposition, the working current and voltage of the ALIS was 0.2 A and 1200 V, respectively. The distance between ALIS and substrate was 130 mm. The DC pulsed bias of −100 V was applied to the substrates during all deposition process. The working current of the DCMS was changed from 0.8 A, 1.0 A, 1.2 A, 1.5 A, 2.0 A to 2.5 A to regulate the doped Cu content in amorphous DLC matrix. The deposition time was controlled to obtain the same thickness (200 ± 30 nm) of films.

### *2.2. Characterization*

The thickness of Cu-DLC films was determined by measuring the step height using a surface profilometer (Alpha-Step IQ, US). Here, a mask was used to cover part of the Si substrate, so some uncoated area of the samples can be obtained.

The chemical compositions and chemical bonds of Cu-DLC films were characterized by X-ray photoelectron spectroscopy (XPS, Axis ultradld, Japan); the test areas were first etched by $Ar^+$ ion of 5 kV for 4 min to remove any oxide from the surface. By integrating the $sp^2$-C peak and $sp^3$-C peak areas which were obtained by Gaussian and Lorentzian mixing functions, the carbon hybridization ratio of $sp^2/(sp^2 + sp^3)$ could be inferred [18,19]. The carbon atomic bonding structure of Cu-DLC films was analyzed by Raman spectroscopy (Renishaw in Via-reflex, 532 nm). The phase structure of Cu-DLC films was characterized by X-ray diffractometer (XRD, D8 ADVANCE, Germany) with Cu Kα radiation, and samples deposited on zero background holders were selected for

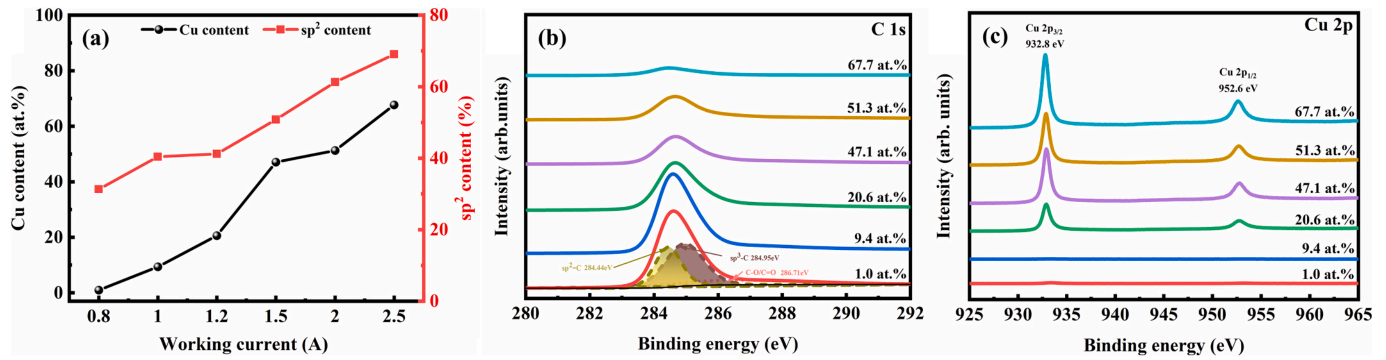


**Fig. 2.** XPS spectra of (a) Cu and $sp^2$ content with different working current of Cu-DLC films according to Gaussian fitting of the C 1s peaks, (b) C 1s peak and (c) Cu 2p on the surface of Cu-DLC films with different Cu contents.

analysis. Transmission electron microscopy (TEM, Talos F200X, US) with an operating voltage of 200 kV was used to study the microstructure of Cu-DLC films. The sample for TEM observation was prepared by Focused Ion Beam (FIB) instrument (Carl Zeiss, Auriga).

The Cu-DLC piezoresistors for test were deposited on silicon oxide substrates, with the dimension of 35 × 5 × 0.5 mm. The conductive silver paste was used at both ends of the test sample to lead out the copper wires, and the resistance was measured by a desktop multimeter (FLUKE, 8846A) during the test. The GF was measured by a home-made three-point bending equipment according to the following formula [20]. The specific conditions of the equipment were detailed in [21].

$$GF = \frac{\Delta R}{R \bullet \varepsilon} = \frac{l^2}{3t \bullet \Delta Y} \bullet \frac{\Delta R}{R} \quad (1)$$

where R is the nominal resistance, ΔR is the change of resistance under applied strain, ε is strain measured by formula $(3t \bullet \Delta Y)/l^2$, t is the thickness of the pristine substrate sample, taken as 0.5 mm, $l$ is the length between two fulcrums, ΔY is the deflection.

The physical property measurement system (PPMS, PPMS-DynaCool, US) was used to measure the I-V characteristic and electrical resistivity of Cu-DLC films with a temperature range from 100 to 350 K. The test samples were deposited on $Al_2O_3$, with the size of 7 × 2.5 × 0.5 mm. Besides, their spatial distribution of current paths and local electrical properties were also characterized via a conductive atomic force microscope (C-AFM), with scan rate 2.0 Hz, working voltage 1 V, scan area 1 × 1 μm and resolution 512 × 512 pixels.

## 3. Result

### 3.1. Thickness, chemical composition and structure

To eliminate the influence of film thickness on their electrical performance, the thickness of the Cu-DLC films was controlled at 200 ± 30 nm by adjusting the deposition time. With the sputtering current increasing from 0.8 to 2.5 A, the deposition rate of Cu-DLC increased from 13.9 to 68.0 nm/min, this could be explained by the higher sputtering yield of Cu at a higher incident energy of $Ar^+$ [22].

Fig. 2 shows the XPS spectra and the fitting results of the Cu-DLC films with different working currents. In Fig. 2(a), with the working current increasing from 0.8 to 2.5 A, the Cu content increased from 1.0 to 67.7 at.%, the $sp^2$ content also increased from 31.3 to 69.1 %, which suggested that the doped Cu atoms were beneficial to the formation of $sp^2$ phase, as reported in former research [23,24]. Fig. 2(b) shows the C 1s spectra of the Cu-DLC films with different Cu contents. The C 1s peaks intensity decreased with increasing Cu content due to the reduction of C content. All the C1s spectra displayed asymmetric peaks, which could be fitted using three components corresponding to $sp^2$-C, $sp^3$-C and C-O/C=O bonds, separately [16,25]. A few O element might be from the residual oxygen in the vacuum chamber or the atmospheric environment [16]. Besides, from Cu 2p spectra in Fig. 2(c), when the Cu content exceeded 9.4 at.%, Cu $2p_{3/2}$ peak around 932.8 eV and Cu $2p_{1/2}$ around 952.6 eV appeared, which confirmed the existence of metallic Cu in the amorphous carbon matrix [26].

Fig. 3(a) illustrates the Raman spectra of the Cu-DLC films with different Cu contents. All films showed typical asymmetric peaks of amorphous carbon, in the wave number range of 800 to 2000 $cm^{-1}$ [27]. The Raman spectra could be fitted into the D and G peaks near 1360 and

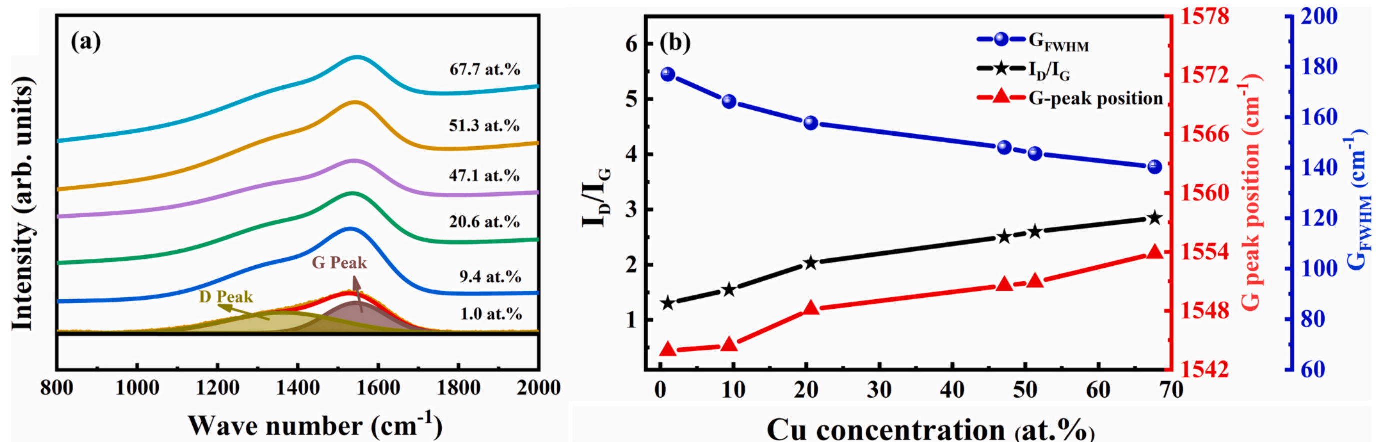


**Fig. 3.** (a) Raman spectra, (b) $I_D/I_G$, G peak position and $G_{FWHM}$ of Cu-DLC films with different Cu contents deposited on Si.

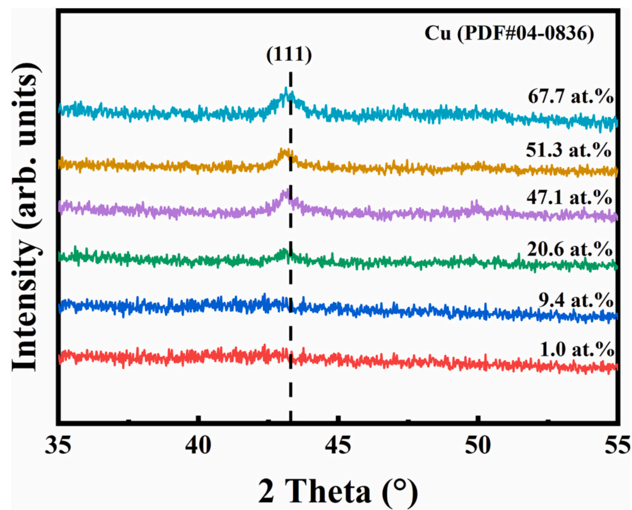


**Fig. 4.** XRD patterns of Cu-DLC films.

1550 cm$^{-1}$ respectively, with two Gaussian fitting method [28,29]. From the full width at half maximum of the G peak ($G_{FWHM}$), the peak area ratio of D peak to G peak ($I_D/I_G$) and the G-peak position, the size and distribution of the sp$^2$ clusters can be qualitatively analyzed [30,31]. Fig. 3(b) presents the $G_{FWHM}$, $I_D/I_G$ and the G-peak position with different Cu contents. As the Cu content increased from 1.0 to 67.7 at.%, the $I_D/I_G$ ratio increased from 1.3 to 2.85 and the G peak position showed a hypsochromic shift from 1543.9 to1553.8 cm$^{-1}$, which indicated the increase of the sp$^2$/sp$^3$ ratio and sp$^2$ cluster size, separately [32]; meanwhile, the $G_{FWHM}$ decreased from 177 to 140.4 cm$^{-1}$, which indicated a reduced structural disorder.

Fig. 4 presents the XRD patterns of Cu-DLC films with different Cu contents. No diffraction peaks appeared for samples with Cu content less than 9.4 at.%. With 20.6 at.% Cu, a weak diffraction peak near 2θ = 43.3° can be observed, which was identified as the (111) crystal plane of the face-centered cubic (FCC) copper phase (PDF 04–0836). With the increase of the Cu content to 67.7 at.%, the intensity of Cu (111) gradually increased.

Fig. 5 shows the high-resolution TEM (HRTEM) micrograph and corresponding SAED of Cu-DLC with 9.4 and 20.6 at.% Cu. With 9.4 at.% Cu, a certain amount of nanoparticulates were distributed in amorphous carbon matrix, and most of the nanoparticulates were with the diameter of 5 to 10 nm, as shown in Fig. 5(a). Compared with the HRTEM and SAED, the interplanar spacing of the nanocrystal could match well with the FCC Cu, and the (111), (200), (220) and (311) reflections were identified. In Fig. 5(b), more and larger Cu nanoparticulates appeared with 20.6 at.% Cu. Similarly, Dai et al. proposed that the Cu nanoparticulates could only emerge once the doped Cu content exceeded a threshold value. Otherwise, the doped Cu atoms would be dissolved uniformly in the amorphous DLC matrix [33]. This was consistent with the results obtained by Meškinis et al. reported similar results [3]. Combined with the previous XPS and XRD result, it can be concluded that in the Cu-DLC films with higher Cu content, Cu nanoparticulates will be formed and separated by the amorphous carbon matrix.

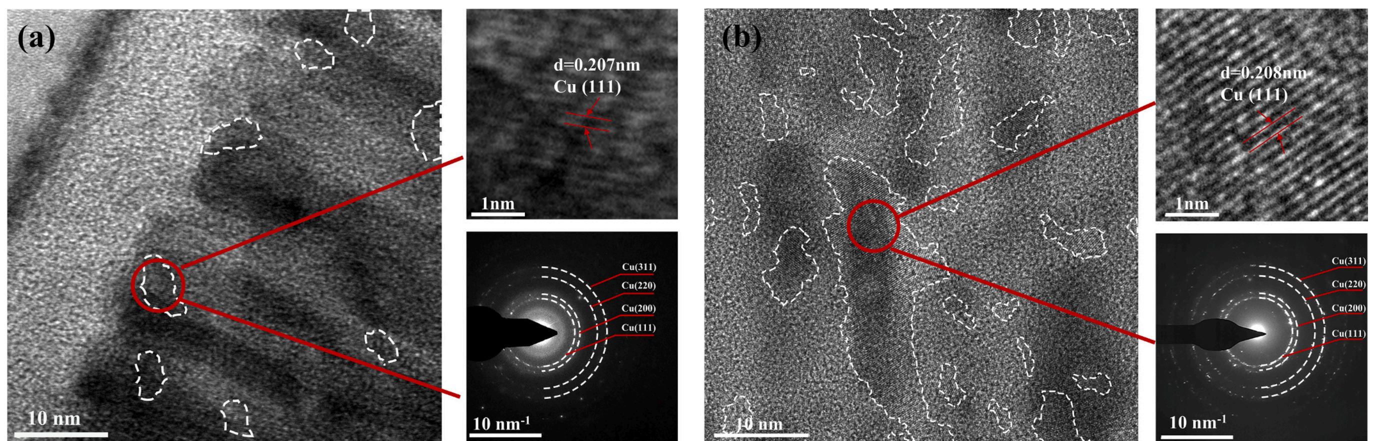


**Fig. 5.** HRTEM image and corresponding SAED of Cu-DLC film with (a) 9.4 at.% and (b) 20.6 at.% Cu.

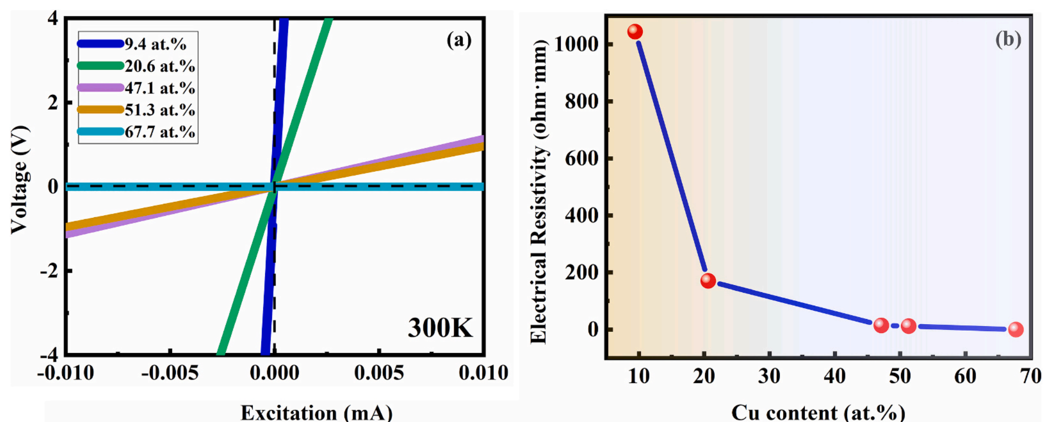


**Fig. 6.** (a) I-V characteristic plots and (b) electrical resistivity at 300 K of the Cu-DLC films deposited with different Cu contents.

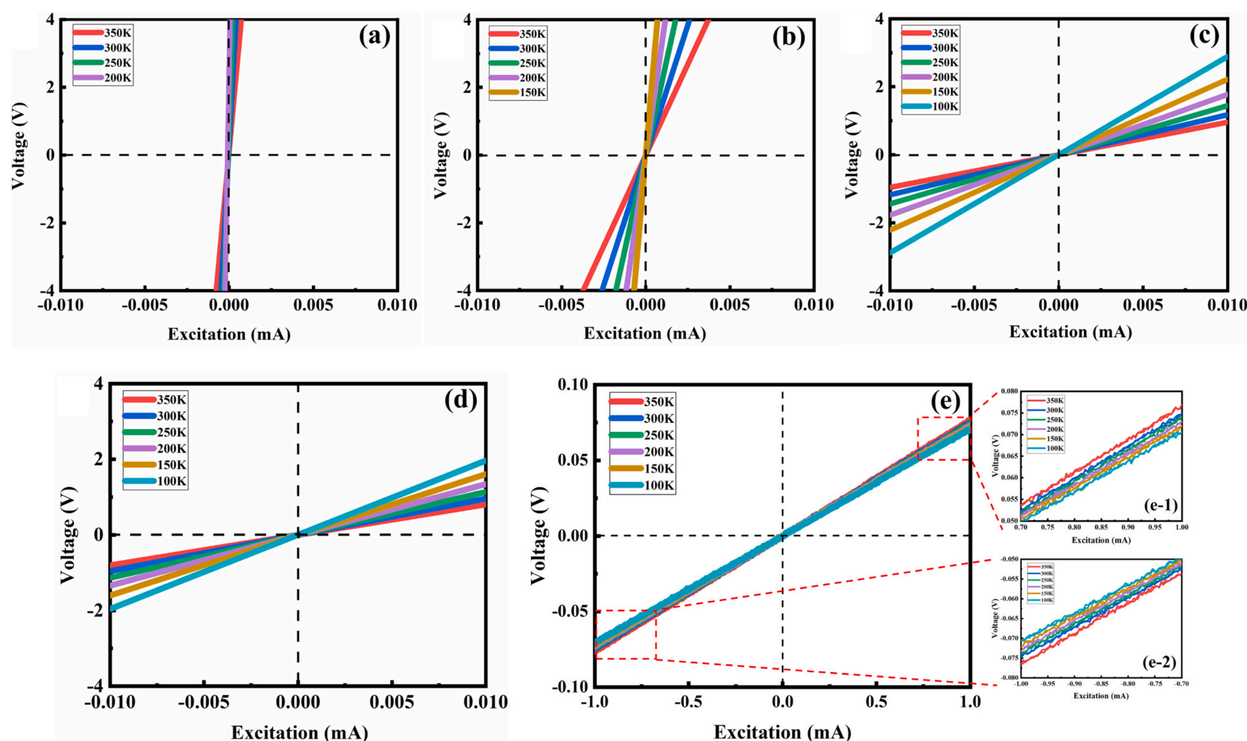


**Fig. 7.** I-V plots of the Cu-DLC films deposited with (a) 9.4, (b) 20.6, (c) 47.1, (d) 51.3, (e) 67.7 at.% Cu content from 100 to 350 K.

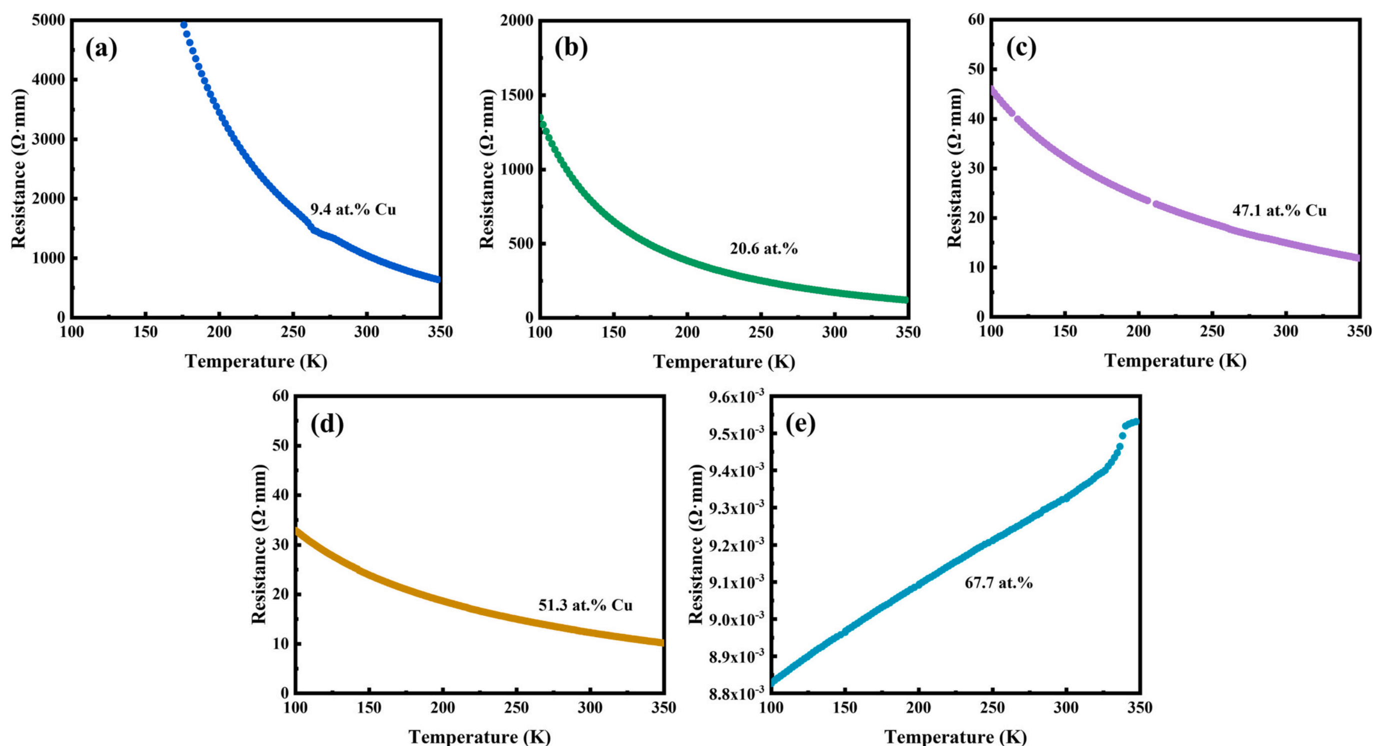


**Fig. 8.** R-T behaviors of Cu-DLC films deposited with (a) 9.4, (b) 20.6, (c) 47.1, (d) 51.3, (e) 67.7 at.% Cu.

### *3.2. Electrical properties*

Fig. 6 shows I-V characteristic plots and electrical resistivity (R) of Cu-DLC films. I-V of the sample with 1.0 at.% Cu was not displayed here, since its resistance exceeded the upper limit of the instrument test range. For samples with Cu content from 9.4 to 67.7 at.%, the voltage was positively linear correlated with the excitation from −0.01 to 0.01 mA, suggesting their typical ohmic behavior. According to the I-V characteristic plots in Fig. 6(a), the corresponding R of Cu-DLC films was shown in Fig. 6(b). As the Cu content increased from 9.4 to 67.7 at.%, R decreased monotonically from 1044.8 to $9.3 \times 10^{-3}$ Ω·mm, due to the increase of conductive phase content.

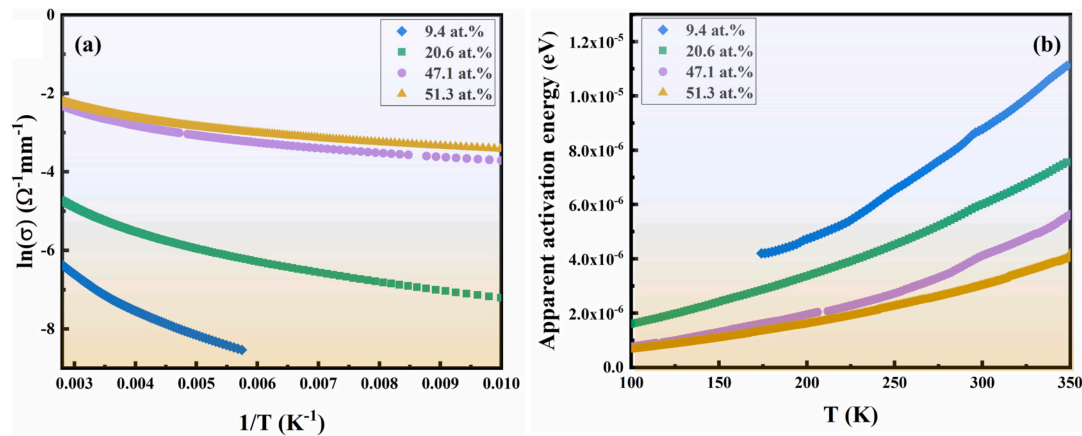


**Fig. 9.** (a) Temperature dependence of conductivity and (b) apparent activation energy for Cu-DLC films deposited with different Cu contents.

For Cu-DLC films with 9.4, 20.6, 47.1, 51.3, 67.7 at.% Cu content, their I-V plots from 100 to 350 K were also depicted in Fig. 7. Similarly, for some Cu-DLC samples, their resistance can exceed the upper limit of the instrument under certain temperature, some I-V plots are not provided. All test samples displayed excellent linear I-V behavior. At a certain temperature, the sample with higher Cu content showed a smaller voltage value under the same excitation current, that was, the sample with higher Cu content exhibited a lower resistance. Besides, for each test sample with Cu content less than 67.7 at.%, under the same excitation current, its corresponding voltage value decreased with increasing the test temperature, which indicated their typical semiconductor behavior, as shown in Fig. 7(a-d). While, for Cu content at 67.7 at.%, the electrical resistance increased with the increase of the test temperature, suggesting a typical metal-like conductive behavior, as shown in Fig. 7(e).

Fig. 8 presents temperature dependence of resistivity (R-T) of Cu-DLC films in the temperature range of 100 to 350 K. For the samples with Cu content less than 51.3 at.%, the resistance decreased monotonically with the increase of temperature, and for sample with lower Cu content, its resistivity showed stronger dependency on the test temperature. For example, the resistance of sample with 20.6 at.% copper increased significantly from 119.2 to 1349.4 Ω·mm, with the temperature decreasing from 350 to 100 K; for the sample with 51.3 at.% copper, its resistance only increased around three times, from 10.1 Ω·mm at 350 K to 32.9 Ω·mm at 100 K. While, for the sample with 67.7 at.% Cu, its resistance decreased slightly from $9.53 \times 10^{-3}$ Ω·mm at 350 K to $8.83 \times 10^{-3}$ Ω·mm at 100 K.

To further explore the underlying transport mechanism, their resistivity R and test temperature T of the samples with various Cu were fitted. First, their temperature dependence of conductivity was analyzed by activation energy via simple Arrhenius law [13,34]:

$$E = -k[d\ln(\sigma)/d(1/T)] \quad (2)$$

where E is the apparent activation energy, σ is the conductivity, that is the multiplicative inverse of resistivity, k is Boltzmann constant, T is test temperature.

The ln(σ)-(1/T) curves of samples with typical semiconductor characteristics are shown in Fig. 9(a), and curves below 174 K for 9.4 at.% Cu sample is not displayed, due to its large resistance. Obviously, all ln(σ)-(1/T) curves exhibited nonlinear characteristic. From the slope of the curves, the E was calculated, as shown in Fig. 9(b). The sample with larger amount of Cu content displayed a smaller E value due to the compensation effect of metal on semiconductor. And all the E value evidently increased with increasing temperature. For instance, E

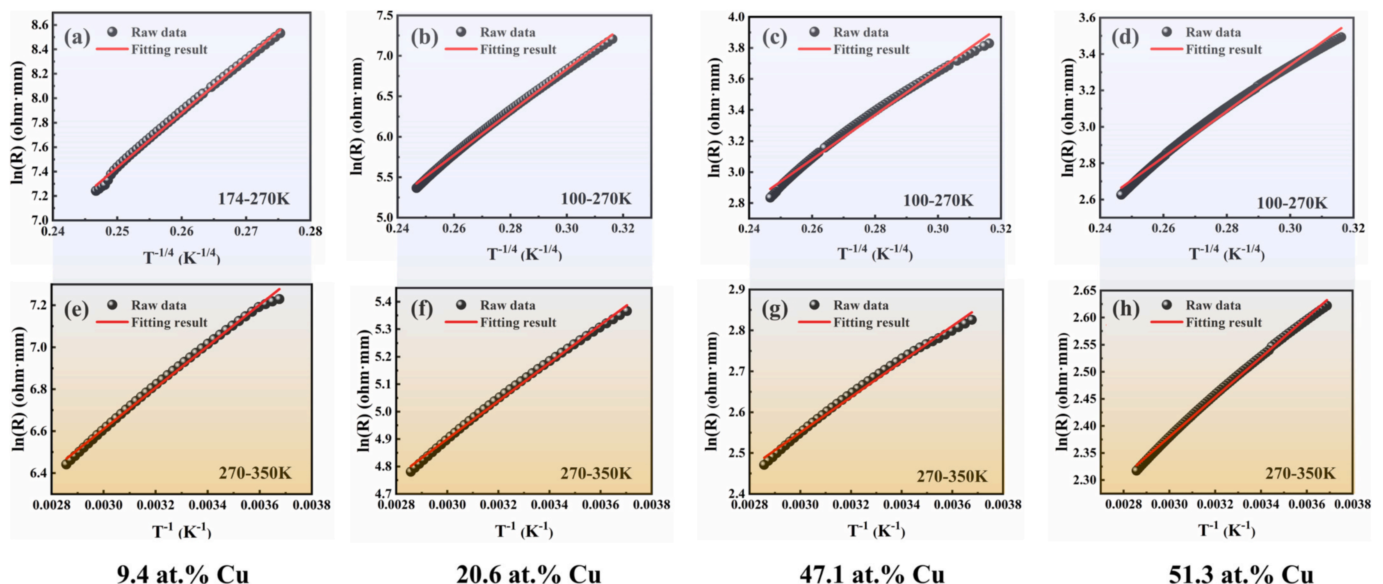


**Fig. 10.** Relationship between ln(R) and $T^{-1/4}$ (a), (b), (c), (d) and $T^{-1}$ (e), (f), (g), (h) at different temperature ranges for the sample with 9.4, 20.6, 47.1, 51.3 at.% Cu content. The red lines are fitting results.

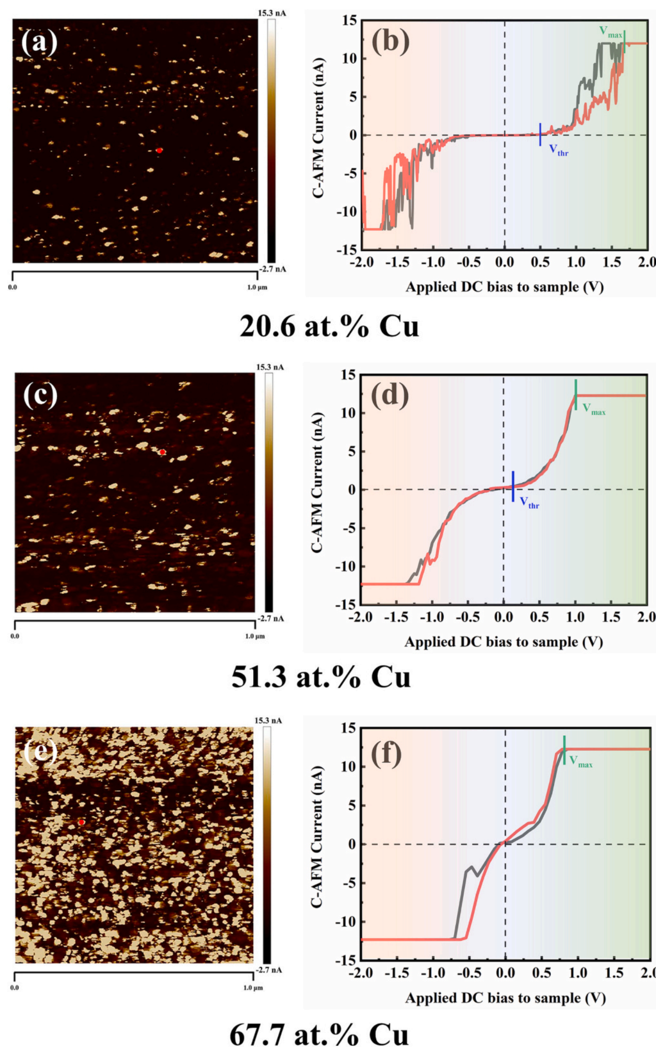


**Fig. 11.** The current images and corresponding I-V plots for the sample with 20.6 at.% Cu (a), (b); 51.3 at.% Cu (c), (d) and 67.7 at.% Cu (e), (f).

increased from $1.59 \times 10^{-6}$ eV at 100 K to $7.63 \times 10^{-6}$ eV at 350 K for the sample with 20.6 at.% copper. This change of activation energy with temperature suggested that the simple Arrhenius law cannot explain their transport behavior in the whole test temperature range.

According to the previous XPS, XRD and TEM, Cu nanoparticulates were distributed in the amorphous carbon matrix, the Cu-DLC films could be simplified as composite where conductive $sp^2$ cluster and Cu phase were separated by the insulating $sp^3$ matrix [35,36], and their electrical properties could be explained from the tunneling process between isolated conductive phase. The resistivity R and test temperature T of the Cu-DLC film were fitted at different temperature ranges, as shown in Fig. 10, according to the following formula [37]:

$$R = R_0 exp(T_0/T)^n \tag{3}$$

where $R_0$ is a pre-exponential index, $T_0$ is a characteristic temperature which depends on the localization length and density of states, n {=1/(d + 1)} taking different values is used to indicate the change of electron transport mechanism and the hopping dimensionality. And d is the hopping dimensionality, whose value can be taken as 1, 2 or 3, corresponding to one-, two- or three-dimensional tunneling process, respectively. Electron transport mechanism is thermal activation when n equals 1, or Mott-type variable range hopping (VRH) when n equals 1/2, 1/3 or 1/4.

Since the designed thickness of the Cu-DLC films was at least several ten times larger than the size of conductive Cu nanocrystal and $sp^2$ cluster [30], the three-dimensional tunneling process might be suitable in this case [38]. In Fig. 10(a), (b), (c), (d), the ln(R) exhibited an obvious linear relationship with $T^{-1/4}$ in the temperature range from 100 K to 270 K; and in the higher temperature range from 270 K to 350 K, the ln($R$)-(1/T) curve showed excellent linear relationship, as shown in Fig. 10(e), (f), (g), (h). The results indicated that thermal activation was the main transport mechanism in the higher temperature range from 270 K to 350 K, while in the low temperature range, three-dimensional Mott-type VRH conduction played a primary role.

To explore their local electrical properties, three Cu-DLC samples with 20.6 at.%, 51.3 at.% and 67.7 at.% Cu content were characterized by C-AFM. In Fig. 11(a), (c), (e), the brightness of different areas in the images could reflect its conductivity, that was, the brighter area had a higher conductivity. With increasing Cu content, both the signal intensity and size of the local electrical area were enhanced significantly. Besides, the corresponding I-V behavior of the local electrical area for each sample was analyzed, as shown in Fig. 11(b), (d), (f). The I-V curves of the typical bright spots were obtained by ramping the bias voltage from −2 to +2 V. In order to ensure the accuracy of the test data, both forward and reverse bias voltages were applied to the sample. All the I-V curves showed good repeatability and high symmetry. In Fig. 11(b) and (d), the threshold voltage ($V_{thr}$) at 0.5 V and 0.2 V could be identified in the I-V curves, separately, namely, nearly no current could be detected when the bias voltage was less than $V_{thr}$, and when the bias voltage exceeded $V_{thr}$, the current increased significantly. The decreased $V_{thr}$ with the increase of Cu content from 20.6 to 51.3 at.%, indicated that the carrier transport mode can be the tunneling process and the energy required for carrier tunneling decreased with more conductive phase. In Fig. 11(f), no typical threshold voltage was present at 67.7 at.% Cu content. Meanwhile, for each sample, there was a limiting voltage $V_{max}$, when the applied voltage was higher than $V_{max,}$ the current would exceed the upper limit of the equipment. And the $V_{max}$ decreased gradually from around 1.7, 1.0 to 0.8 V with the increase of Cu content from 20.6, 51.3 to 67.7 at.%, which could be explained from the decreased separation distance between neighbouring conductive phase and the gradual formation of conductive paths.

### 3.3. *Piezoresistive behavior*

Both TCR and GF of the Cu-DLC films depended on their chemical composition and microstructure. Based on the XPS and Raman results, both the $sp^2$ content and $sp^2$ cluster size in the Cu-DLC films increased with increasing Cu content. Besides, from the XRD and TEM, Cu nanoparticulates were formed at higher Cu content, the Cu-DLC can be regarded as a composite, which was composed of insulating $sp^3$ matrix and conductive $sp^2$ phase and Cu phase. The carrier tunneling process in this system could be explained by percolation-tunneling theory [3]. The conductivity has a typical power-law relationship with the volume of conductive phase [38,39]:

$$\sigma \propto (x - x_c)^t \tag{4}$$

where $\sigma$ is conductivity, $x$ is the volume fraction of conductive phase, $x_c$ is the threshold, and t is a universal transport exponent. For $x < x_c$, isolated conductive phases existed in the insulating matrix, and the conductivity was attributed to interphase tunneling. While, for $x > x_c$, a continuous network was formed through the connection of conductive phases. As a result, the electric current flowed the film through conductive paths, and the electrical properties could be changed from typical semiconductor to metal-like behavior.

The TCR of the Cu-DLC films refers to the relative change of resistance value when the unit temperature changes, it can be evaluated according to the following formula [40],

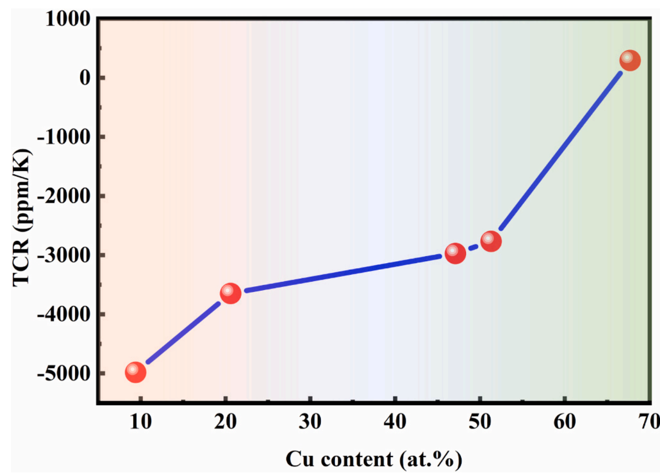


**Fig. 12.** TCR of Cu-DLC films deposited with different Cu contents.

$$TCR = \frac{R_1 - R_0}{R_0} \times \frac{1}{T_1 - T_0} \times 10^6 \tag{5}$$

where $R_1$ and $R_0$ are the resistance of the sample at $T_1 = 350$ K and $T_0 = 100$ K, respectively, as shown in Fig. 12.

With Cu content 9.4 at.%, the sample exhibited a large negative TCR about −4980 ppm/K. With Cu content increasing to 20.6, 47.1 and 51.3 at.%, the TCR was still negative, but its absolute value evidently decreased to −3646, −2971 and −2766 ppm/K, respectively. While, at 67.7 at.% Cu content, the sample showed a positive TCR value of approximately +294 ppm/K. The electrical properties were changed from the typical semiconductor to metal-like behavior, indicating the transport mechanism changed from tunneling to percolation.

Besides, from the ln($R$)-$(1/T)^n$ relationship, thermal activation and three-dimensional Mott-type VRH conduction were identified in high and low temperature ranges, respectively. Combined with the I-V curves from the C-AFM test, the threshold voltage $V_{thr}$ was identified, which suggested the tunneling process between conductive phase at lower Cu content. And with 67.7 at.% Cu content, some conductive phase may be connected with each other and the $V_{thr}$ also disappeared.

In this case, a simple carrier transport model for the electrical properties and piezoresistive effect of the Cu-DLC films was proposed, as shown in Fig. 13. Since conductive $sp^2$ phase and Cu phase were distributed in the insulating $sp^3$ matrix, the reduced distance between the conductive phase might result in trivial change of the tunneling process under the applied strain.

According to thick-film resistors (TFRs) and tunneling process, the gauge factor can be equivalently described by the following equation [41]:

$$GF \equiv \frac{\Delta R}{R \bullet \varepsilon} \simeq \frac{2d}{\xi} \tag{6}$$

where d is a mean distance of adjacent conductive phase, $\xi$ is the localization length. GF decreased evidently from 5.6 to 1.4 with the increase of Cu content as shown in Fig. 14. Combined with the C content from XPS and carbon atomic bonding structure from Raman, it was safe to conclude that the GF of Cu-DLC was inversely proportional to the content of conductive phase. The mechanism of carrier transport was dependent on the distance $d$ of adjacent conductive phases, where the percolation transport would become the dominated mechanism once $d$ was less than 1 nm [42], causing the GF value similar to that of metal. With increasing $d$, the carrier transport was changed to the tunneling transport, and GF was proportional to $d$ under the condition [43]. In this work, the Cu-DLC film with high Cu content will show a weaker piezoresistive effect, due to the reduced distance of adjacent conductive phase.

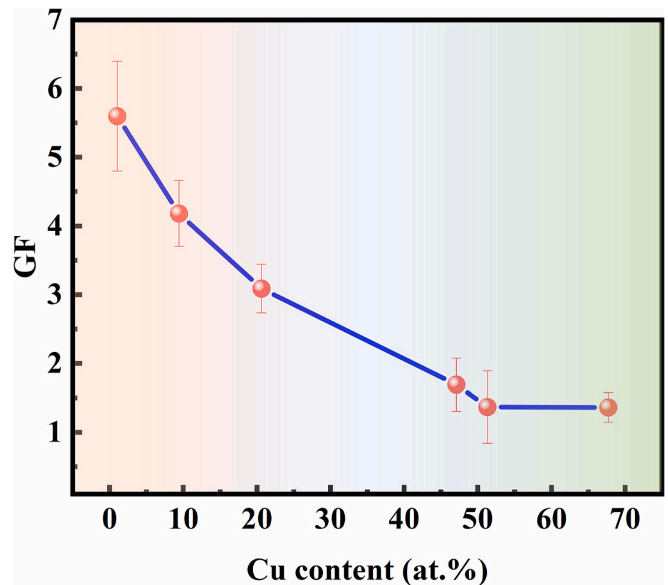


**Fig. 14.** GF testing result of the Cu-DLC films with different Cu contents.

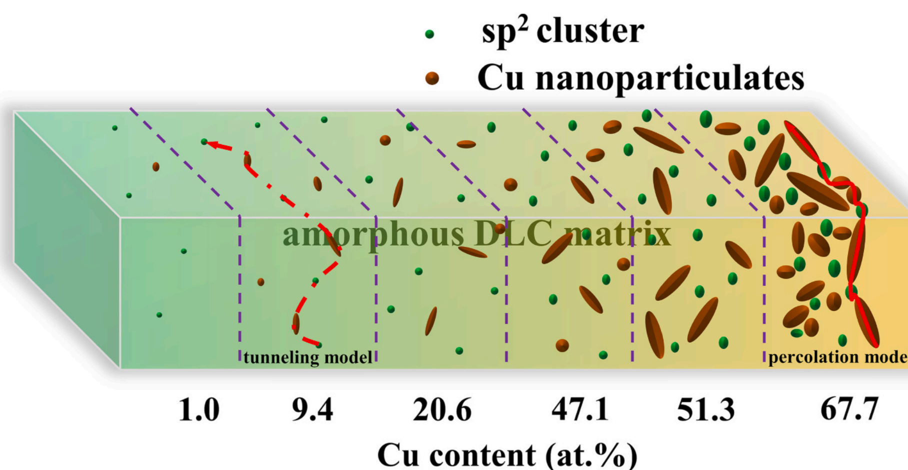


**Fig. 13.** Schematic of carrier transport mechanism of Cu-DLC films with different Cu contents.

## 4. Conclusion

With Cu content increasing from 1.0 to 67.7 at.%, more conductive $sp^2$ phase and Cu phase appeared in Cu-DLC films. The GF decreased evidently from 5.6 to1.4, and their resistivity also decreased monotonically. Especially, from 9.4 to 51.3 at.% Cu content, the Cu-DLC exhibited the semiconductor behavior with negative TCR from −4980 to −2766 ppm/K. They followed thermal activation transport mechanism within the higher temperature range from 270 K to 350 K, and three-dimensional Mott-type VRH conduction within the low temperature range from 100 K to 270 K, respectively. At 67.7 at.% Cu, the sample showed the typical metal-like behavior, with a positive TCR of 294 ppm/K. Combined with the threshold voltage $V_{thr}$ identified by C-AFM test, the carrier tunneling process between conductive phase in the insulating $sp^3$ matrix could explain the electrical properties and piezoresistive effect of the Cu-DLC. These results could provide new insights into the development of high-performance carbon-based piezoresistive film sensors.

### CRediT authorship contribution statement

**Chunliang Yan:** Formal analysis, Data curation, Writing – original draft. **Peng Guo:** Formal analysis, Writing – review & editing. **Jingyuan Zhou:** Investigation. **Rende Chen:** Investigation. **Aiying Wang:** Writing – review & editing, Validation, Project administration, Funding acquisition.

### Declaration of competing interest

The authors declare that they have no known competing financial interests or personal relationships that could have appeared to influence the work reported in this paper.

### Data availability

Data will be made available on request.

### Acknowledgements

This research was supported by the National Natural Science Foundation of China (U20A20296), Science and Technology Innovation 2025 Major Project of Ningbo (2020Z023), Natural Science Foundation of Zhejiang Province (LGG22E010011) and Natural Science Foundation of Ningbo (2021J227).

### References

[1] S. Bhowmick, S. Shirzadian, A.T. Alpas, High-temperature tribological behavior of Ti containing diamond-like carbon coatings with emphasis on running-in coefficient of friction, Surf. Coat. Technol. 431 (2022), 127995, https://doi.org/10.1016/j.surfcoat.2021.127995.
[2] H. Khanmohammadi, W. Wijanarko, S. Cruz, M. Evaristo, N. Espallargas, Triboelectrochemical friction control of W- and Ag-doped DLC coatings in water-glycol with ionic liquids as lubricant additives, RSC Adv. 12 (2022) 3573–3583, https://doi.org/10.1039/d1ra08814a.
[3] S. Meskinis, R. Gudaitis, A. Vasiliauskas, A. Ciegis, K. Slapikas, T. Tamulevicius, M. Andrulevicius, S. Tamulevicius, Piezoresistive properties of diamond like carbon films containing copper, Diam. Relat. Mater. 60 (2015) 20–25, https://doi.org/10.1016/j.diamond.2015.10.007.
[4] T. Takeno, H. Miki, T. Sugawara, Y. Hoshi, T. Takagi, A DLC/W-DLC multilayered structure for strain sensing applications, Diam. Relat. Mater. 17 (2008) 713–716, https://doi.org/10.1016/j.diamond.2007.10.005.
[5] R. Koppert, D. Goettel, O. Freitag-Weber, G. Schultes, Nickel containing diamond like carbon thin films, Solid State Sci. 11 (2009) 1797–1800, https://doi.org/10.1016/j.solidstatesciences.2009.04.022.
[6] S. Meskinis, R. Gudaitis, K. Slapikas, A. Vasiliauskas, A. Ciegis, T. Tamulevicius, M. Andrulevicius, S. Tamulevicius, Giant negative piezoresistive effect in diamond-like carbon and diamond-like carbon-based nickel nanocomposite films deposited by reactive magnetron sputtering of Ni target, ACS Appl. Mater. Interfaces 10 (2018) 15778–15785, https://doi.org/10.1021/acsami.7b17439.
[7] S. Meskinis, A. Vasiliauskas, K. Slapikas, R. Gudaitis, M. Andrulevicius, A. Ciegis, G. Niaura, R. Kondrotas, S. Tamulevicius, Bias effects on structure and piezoresistive properties of DLC:Ag thin films, Surf. Coat. Technol. 255 (2014) 84–89, https://doi.org/10.1016/j.surfcoat.2014.01.026.
[8] S. Tamulevicius, S. Meskinis, K. Slapikas, A. Vasiliauskas, R. Gudaitis, M. Andrulevicius, A. Tamuleviciene, G. Niaura, Piezoresistive properties of amorphous carbon based nanocomposite thin films deposited by plasma assisted methods, Thin Solid Films 538 (2013) 78–84, https://doi.org/10.1016/j.tsf.2012.11.122.
[9] R. Gudaitis, S. Meskinis, K. Slapikas, M. Andrulevicius, G. Niaura, S. Tamulevicius, Piezoresistive and electrical properties of Cr containing diamond-like carbon films, Surf. Coat. Technol. 211 (2012) 80–83, https://doi.org/10.1016/j.surfcoat.2011.08.040.
[10] G. Leal, G.W.A. Cardoso, A.S.D. Sobrinho, M. Massi, Electrical and structural characterization of Sn-DLC thin films for piezoresistive sensors, in: 28th European Conference on Solid-State Transducers (Eurosensors) 87, 2014, pp. 120–123, https://doi.org/10.1016/j.proeng.2014.11.398.
[11] N.F. Mott, E.A. Devis, Electronic processes in non-crystalline materials, Phys. Today 12 (1972) 55, https://doi.org/10.1063/1.3071145.
[12] X. Ma, P. Guo, X.S. Tong, Y.L. Zhao, Q. Zhang, P.L. Ke, A.Y. Wang, Piezoresistive behavior of amorphous carbon films for high performance MEMS force sensors, Appl. Phys. Lett. 114 (2019), 253502, https://doi.org/10.1063/1.5096225.
[13] H. Li, P. Guo, D. Zhang, R.D. Chen, X. Zuo, P.L. Ke, H. Saito, A.Y. Wang, Influence of deposition temperature on the structure, optical and electrical properties of a-C films by DCMS, Appl. Surf. Sci. 503 (2020), 144310, https://doi.org/10.1016/j.apsusc.2019.144310.
[14] R. Koppert, S. Uhlig, H. Schmid-Engel, D. Gottel, A.C. Probst, G. Schultes, U. Werner, Structural and physical properties of highly piezoresistive nickel containing hydrogenated carbon thin films, Diam. Relat. Mater. 25 (2012) 50–58, https://doi.org/10.1016/j.diamond.2012.01.031.
[15] A. Tibrewala, E. Peiner, R. Bandorf, S. Biehl, H. Luthje, Longitudinal and transversal piezoresistive effect in hydrogenated amorphous carbon films, Thin Solid Films 515 (2007) 8028–8033, https://doi.org/10.1016/j.tsf.2007.03.046.
[16] P. Guo, X.W. Li, L.L. Sun, R.D. Chen, P.L. Ke, A.Y. Wang, Stress reduction mechanism of diamond-like carbon films incorporated with different cu contents, Thin Solid Films 640 (2017) 45–51, https://doi.org/10.1016/j.tsf.2017.09.001.
[17] X.W. Li, D. Zhang, K.-R. Lee, A.Y. Wang, Effect of metal doping on structural characteristics of amorphous carbon system: a first-principles study, Thin Solid Films 607 (2016) 67–72, https://doi.org/10.1016/j.tsf.2016.04.004.
[18] J. Wei, P. Guo, H. Li, P.L. Ke, A.Y. Wang, Insights on high temperature friction mechanism of multilayer ta-C films, J. Mater. Sci. Technol. 97 (2022) 29–37, https://doi.org/10.1016/j.jmst.2021.04.028.
[19] J.H. Liang, Z. Milne, M. Rouhani, Y.-P. Lin, R.A. Bernal, T. Sato, R.W. Carpick, Y. R. Jeng, Stress-dependent adhesion and sliding-induced nanoscale wear of diamond-like carbon studied using in situ TEM nanoindentation, Carbon 193 (2022) 230–241, https://doi.org/10.1016/j.carbon.2022.03.030.
[20] Y.L. He, X.H. Wu, H.Y. Lin, H. Wang, C. Li, Structure characteristics and piezoresistive effect of nc-Si: H films, Chin. Sci. Bull. 40 (1995) 1684–1687.
[21] X. Ma, Q. Zhang, P. Guo, X.S. Tong, Y.L. Zhao, A.Y. Wang, MEMS pressure sensor based on piezoresistive effect of amorphous carbon film, Surf. Technol. 49 (2020) 60–67, https://doi.org/10.16490/j.cnki.issn.1001-3660.2020.06.007.
[22] M. Chen, J. Wang, C.Q. Chen, Z. Liu, Calculation and analysis based on Sigmund's theory for sputtering yield, Vacuum 44 (2007) 44–47, https://doi.org/10.3969/j.issn.1002-0322.2007.02.011.
[23] B. Zhou, Z.B. Liu, D.G. Piliptsou, S.W. Yu, Z.F. Wang, A.V. Rogachev, A. S. Rudenkov, A. Balmakou, Structure and optical properties of Cu-DLC composite films deposited by cathode arc with double-excitation source, Diam. Relat. Mater. 69 (2016) 191–197, https://doi.org/10.1016/j.diamond.2016.09.004.
[24] J. Zhang, S. Zhou, Y. Wang, Y. Wang, C. Wang, X. Lu, C. Mao, S. Chen, X. Lu, L. Wang, Enhancing anti-corrosion and antifouling properties of Cu/GLC composite film for marine application, Surf. Coat. Technol. 375 (2019) 414–426, https://doi.org/10.1016/j.surfcoat.2019.07.054.
[25] Y.L. Gong, P.P. Jing, Y.J. Zhou, Q.Y. Deng, R. Shen, N. Huang, Y.X. Leng, Formation of rod-shaped wear debris and the graphitization tendency of Cu-doped hydrogenated diamond-like carbon films, Diam. Relat. Mater. 102 (2020), 107654, https://doi.org/10.1016/j.diamond.2019.107654.
[26] Y.Y. Liu, M.H. Sun, Y.F. Yuan, Q. Wu, H.X. Wang, Y. He, Z. Lin, F.L. Zhou, M. Ling, C. Qian, C.D. Liang, J. Lu, Accommodation of silicon in an interconnected copper network for robust Li-ion storage, Adv. Funct. Mater. 30 (2020), 1910249, https://doi.org/10.1002/adfm.201910249.
[27] A.C. Ferrari, J. Robertson, Raman spectroscopy of amorphous, nanostructured, diamond-like carbon, and nanodiamond, Philos. Trans. R. Soc. A 362 (2004) 2477–2512, https://doi.org/10.1098/rsta.2004.1452.
[28] A.C. Ferrari, J. Robertson, Interpretation of Raman spectra of disordered and amorphous carbon, Phys. Rev. B 61 (2000) 14095–14107, https://doi.org/10.1103/PhysRevB.61.14095.
[29] N. Aslan, M.S. Kurt, M.M. Koc, Morpho-structural and optoelectronic properties of diamond like carbon-germanium (DLC-Ge) composite thin films produced by magnetron sputtering, Opt. Mater. 126 (2022), 112229, https://doi.org/10.1016/j.optmat.2022.112229.
[30] J. Robertson, Diamond-like amorphous carbon, Mater. Sci. Eng. R. Rep. 37 (2002) 129–281, https://doi.org/10.1016/s0927-796x(02)00005-0.
[31] L. Ji, H.X. Li, F. Zhao, J.M. Chen, H.D. Zhou, Microstructure and mechanical properties of Mo/DLC nanocomposite films, Diam. Relat. Mater. 17 (2008) 1949–1954, https://doi.org/10.1016/j.diamond.2008.04.018.
[32] P.K. Chu, L.H. Li, Characterization of amorphous and nanocrystalline carbon films, Mater. Chem. Phys. 96 (2006) 253–277, https://doi.org/10.1016/j.matchemphys.2005.07.048.

[33] W. Dai, A.Y. Wang, Q.M. Wang, Microstructure and mechanical property of diamond-like carbon films with ductile copper incorporation, Surf. Coat. Technol. 272 (2015) 33–38, https://doi.org/10.1016/j.surfcoat.2015.04.027.

[34] A. Helmbold, P. Hammer, J.U. Thiele, K. Rohwer, D. Meissner, Electrical conductivity of amorphous hydrogenated carbon, Philos. Mag. B 72 (1995) 335–350, https://doi.org/10.1080/13642819508239088.

[35] S. Meskinis, A. Vasiliauskas, K. Viskontas, M. Andrulevicius, A. Guobiene, S. Tamulevicius, Hydrogen-free diamond like carbon films with embedded cu nanoparticles: structure, composition and reverse saturable absorption effect, Materials 13 (2020) 760, https://doi.org/10.3390/ma13030760.

[36] I. Yaremchuk, S. Meskinis, T. Bulavinets, A. Vasiliauskas, M. Andrulevicius, V. Fitio, Y. Bobitski, S. Tamulevicius, Effect of oxidation of copper nanoparticles on absorption spectra of DLC: cu nanocomposites, Diam. Relat. Mater. 99 (2019), 107538, https://doi.org/10.1016/j.diamond.2019.107538.

[37] C.H. Wan, X.Z. Zhang, J. Vanacken, X.L. Gao, X. Zhang, L.H. Wu, X.Y. Tan, H. Lin, V.V. Moshchalkov, J. Yuan, Electro- and magneto-transport properties of amorphous carbon films doped with iron, Diam. Relat. Mater. 20 (2011) 26–30, https://doi.org/10.1016/j.diamond.2010.11.001.

[38] C. Grimaldi, Theory of percolation and tunneling regimes in nanogranular metal films, Phys. Rev. B 89 (2014), 214201, https://doi.org/10.1103/PhysRevB.89.214201.

[39] D. Toker, D. Azulay, N. Shimoni, I. Balberg, O. Millo, Tunneling and percolation in metal-insulator composite materials, Phys. Rev. B 68 (2003), 041403, https://doi.org/10.1103/PhysRevB.68.041403.

[40] M. Petersen, U. Heckmann, R. Bandorf, V. Gwozdz, S. Schnabel, G. Brauer, C. P. Klages, Me-DLC films as material for highly sensitive temperature compensated strain gauges, Diam. Relat. Mater. 20 (2011) 814–818, https://doi.org/10.1016/j.diamond.2011.03.036.

[41] C. Grimaldi, P. Ryser, S. Strassler, Gauge factor enhancement driven by heterogeneity in thick-film resistors, J. Appl. Phys. 90 (2001) 322–327, https://doi.org/10.1063/1.1376672.

[42] M.H. Polley, B.B.S.T. Boonstra, Carbon blacks for highly conductive rubber, Rubber Chem. Technol. 30 (1957) 170–179, https://doi.org/10.5254/1.3542660.

[43] T. Ohno, T. Takeno, H. Miki, T. Takagi, Microstructural design for fabrication of strain sensor utilizing tungsten-doped amorphous carbon coatings, Diam. Relat. Mater. 20 (2011) 651–654, https://doi.org/10.1016/j.diamond.2011.03.003.